Free Radical Biology and Medicine 173 (2021) 97–103

Contents lists available at ScienceDirect

Free Radical Biology and Medicine

journal homepage: www.elsevier.com/locate/freeradbiomed

Study of Carnosine's effect on nude mice skin to prevent UV-A damage

Silvia Radrezza [a], Marina Carini [a], Giovanna Baron [a], Giancarlo Aldini [a], Anne Negre-Salvayre [b], Alfonsina D'Amato [a,*]

[a] Department of Pharmaceutical Sciences, University of Milan, Via L. Mangiagalli 25, 20133, Milan, Italy
[b] Inserm UMR-1048, Toulouse, France, University of Toulouse, Toulouse, France

ARTICLE INFO

Keywords:
Hairless mice skin
UV-A
Carnosine
Quantitative proteomics
Protein networking

ABSTRACT

The skin is an important barrier against external attacks from bacteria, radicals, or radiations. UV-A radiations cause significant impairment of this barrier, inducing inflammation, oxidative stress, and wrinkle formation, thereby promoting photoaging. Previous studies reported that carnosine, a potent antioxidant, and carbonyl scavenger agent, may prevent photoaging features in the skin of hairless mice exposed to UV-A radiations. In the present study, we used a quantitative proteomic approach to analyze the changes evoked by carnosine in the skin proteome of hairless mice exposed to UV-A. This approach allowed to quantify more than 2480 proteins, among them consistent differences were observed for 89 proteins in UV-A exposed *vs* control unexposed skins, and 252 proteins in UV-A-exposed skin preventively treated by carnosine (UVAC) *vs* UV-A. Several functional pathways were altered in the skins of UV-A exposed hairless mice, including the integrin-linked kinase, calcium signaling, fibrogenesis, cell migration and filament formation. An impairment of mitochondrial function and metabolism was observed, with an up-regulation of cytochrome C oxidase 6B1 and NADH: ubiquinone oxidoreductase S8. Skins pre-treated by carnosine were prevented from UV-A induced proteome alterations. In conclusion, our study emphasizes the potency of a proteomic approach to identify the consequences of UV radiations in the skins, and points out the capacity of carnosine to prevent the alterations of skin proteome evoked by UV-A.

1. Introduction

The skin is an efficient defensive barrier against external insults. Nevertheless, long-term ultraviolet (UV) radiation exposure can result in alterations of its structure and functionality *via* direct and indirect effects [1–3]. The solar UV wavebands are mainly constituted by UV-A (315–400 nm) and a small portion of UV-B (280–315 nm) while short-wave UV-C (100–280 nm) are completely absorbed by the stratospheric ozone. UV-A are able to deeply penetrate into the skin dermis up to the basal layer, and are considered as a main cause for skin photoaging [4,5]. Skin photoaging is characterized by the formation of wrinkles, a loss of skin tone and elasticity, dryness, and stiffening [1,2,6,7]. At the molecular and biochemical level, chronic exposure to UV-A progressively leads to a disorganization of the extracellular matrix (ECM), alteration of DNA, dysregulated autophagy, chronic inflammation, alteration of fatty acids, carbohydrates or protein structure, all events involved in skin aging and the increasing of the risk of developing skin cancers [5,8]. The mechanisms leading to skin damages are not fully understood and may derive (at least in part) from the generation of reactive oxygen species (ROS) and subsequent lipid peroxidation [9]; Rabe JH et al., 2016).

We previously reported that lipid peroxidation products such as hydroxynonenal (HNE) and acrolein are generated in the skin dermis of hairless mice chronically exposed to UV-A radiations. These agents form adducts on extracellular matrix components such as elastin, with possible implication in solar elastosis [10]; Rabe JH et al., 2006 [11]). HNE and acrolein may contribute to dermis fibroblast senescence by promoting the expression of senescence markers such as γ- H2AX or the modification of cytoskeletal proteins such as vimentin, in the skin of UV-irradiated hairless mice or in cultured fibroblasts [12]. Many other systems could be affected by ROS or lipid oxidation products generated by UV-A, with consequences on protein function, signaling, antioxidant systems or gene expression.

Several compounds are used to protect the skin against UV radiations, among them antioxidants and carbonyl scavengers [13]; Hughes et al., 2021 [14]]). In this context, we reported that a topical treatment

* Corresponding author.
E-mail addresses: silvia.radrezza@unimi.it (S. Radrezza), marina.carini@unimi.it (M. Carini), giovanna.baron@unimi.it (G. Baron), giancarlo.aldini@unimi.it (G. Aldini), anne.negre-salvayre@inserm.fr (A. Negre-Salvayre), alfonsina.damato@unimi.it (A. D'Amato).

https://doi.org/10.1016/j.freeradbiomed.2021.07.010
Received 10 May 2021; Received in revised form 29 June 2021; Accepted 5 July 2021
Available online 7 July 2021

of the hairless mice skin with carnosine, an endogenous β-alanyl-L-histidine dipeptide with antioxidant and carbonyl scavenger properties, significantly prevented the visible signs of photoaging [15]. At the molecular level, carnosine prevented the modification of elastin as well as the process of fibroblast senescence evoked by HNE or acrolein [10,12]. Carnosine readily reacts with aldehydes like acrolein or HNE to form nonreactive adducts, preventing the process of protein modification and subsequent alteration of cells and tissues [16,17]. It is likely that carnosine treatment exerts a larger scale of protective responses in UV-irradiated skin, and a deeper characterization of its effects may allow a better understanding of skin alterations evoked by UV radiations.

The current development of 'omics sciences (genomics, proteomics, metabolomics etc.) supported by performing analytical tools is showing a new molecular panorama with the availability of a huge amount of data. Proteomic studies represent a suitable technique for analyzing and characterizing the nature and alterations of proteins in various pathophysiological areas [18–20], particularly in the skin [21]. A proteomic atlas of human skin (https://skin.science/) has been established [22]. The quantitative distribution of skin structural proteins, obtained by label free quantitative proteomics, is an important resource for translational research in this area too [22,23]. Dermatological diseases, such as human malignant melanomas [24], eczema [25], psoriasis [26], were characterized by the alteration of proteome in the different states, control versus disease. Moreover, murine skin protein profiling was also described during ageing [27] and in psoriasis-like disease [28]. However, and surprisingly, only few studies were focused on the murine or human skin proteome or its protection by antioxidants and related compounds, upon exposure to UV-radiations.

The present study was designed to provide an in-depth description of the murine skin proteome of hairless mice exposed to UV-A radiations and the preventive effect of carnosine, using a label-free quantitative proteomics approach by high-resolution mass spectrometry. These analyses were carried out on murine skin samples from Negre-Salvayre's previous study showing that carnosine may prevent several photoaging features in the skin of UV-A irradiated hairless mice [10,12].

2. Materials & methods

2.1. Experimental treatment

Skin samples used in this work were from our previous study [10]; experimental protocol N°12/1048/10/13, approved by the French legislation and the local ethical committee for animal experiments). Briefly, this study was carried out on albino hairless mice Skh:hr-1 (8 weeks old, Charles River Laboratories) (4 animals/condition), with one control non-irradiated group, one group daily exposed to UV-A radiations (20 J/cm^2 daily, up to 600 J/cm^2), one group treated with polyethylene glycol (PG) (solvent for carnosine) and daily exposed to UV-A, and one group treated by carnosine (1% in PG) and exposed to UV-A. Carnosine and PG were spread over the back at the end of UV-A exposure. After animal sacrifice, samples of skins from mouse backs were recovered and stored at −80 °C until use [10].

2.2. Sample preparation

Each sample was homogenized by glass bead beating (3 cycles, 60″, 350 rpm) in 100 μL of protein extraction buffer (8 M urea in 50 mM Tris-HCl, 30 mM NaCl (Bio-Rad) at 8.5 pH and 1% of protease inhibitor cocktail (Sigma-Aldrich)). The supernatant was collected in fresh tubes and centrifuged at 14000×*g*, 4 °C for 10 min and sonicated by probe.

The amount of proteins was quantified by the Bradford Reagent (Sigma-Aldrich) following the standard procedure. 20 μg of proteins in 50 mM NH_4HCO_3 were reduced with 5 mM DL-dithiothreitol (DTT, Sigma-Aldrich) for 30 min at 52 °C shaking, then centrifuged at 500 rpm and alkylated with 15 mM iodoacetamide (Sigma-Aldrich) for 20 min in the dark at room temperature. The protein digestion was performed in 1:100 lysC: protein ratio (w/w) for 3 h at 37 °C shaking at 650 rpm followed by 1:20 trypsin:protein ratio (w/w) (Trypsin Sequencing Grade; Roche, Monza, Italy) overnight at 37 °C shaking at 650 rpm.

2.3. High-resolution mass spectrometry analysis (nLC-HRMS)

To increase the quality of instrumental analysis, the digested samples were further purified and concentrated by 0.6 μL C-18 resin ZipTip (Millipore, Milan, Italy). Tryptic peptides were analyzed using a Dionex Ultimate 3000 nano-LC system (Sunnyvale CA, USA) connected to Orbitrap Fusion™ Tribrid™ Mass Spectrometer (Thermo Scientific, Bremen, Germany) equipped with a nano-electrospray ion source (nESI). Peptide mixtures were pre-concentrated onto an Acclaim PepMap 100 - 100 μm × 2 cm C25 and separated on EASY-Spray column, 25 cm × 75 μm ID packed with Thermo Scientific Acclaim PepMap RSLC C18, 3 μm, 100 Å. The temperature was set to 35 °C and the flow rate was 300 nL min^{-1}. Mobile phases were the following: 0.1% formic acid (FA) in water (solvent A), 0.1% FA in water/acetonitrile with 2/8 ratio (solvent B). The elution gradient was from 96% buffer A to 40% buffer B for 110 min. MS spectra were collected over an *m/z* range of 375–1500 Da at 120,000 resolutions, operating in data dependent scan mode, cycle time 3 s between master scans. Higher-energy collision dissociation (HCD) was performed with collision energy set at 35 eV in positive polarity. Each sample was analyzed in three technical replicates.

2.4. Data analysis

The instrumental raw files were processed by MaxQuant software v1.6.6.0 [29] set on the *Uniprot_Homosapiens* database against the Andromeda search engine. The quantification of peptides and related proteins for each control and treated sample in biological duplicate and technical triplicates was based on the LFQ intensities. Lys-C and trypsin as the digestive enzymes, variable modification of carbamidomethylation of cysteine (+57.021 Da), fixed modification of methionine oxidation (+15.995 Da), N-terminal acetylation (+42.011 Da) and LFQ minimum ratio count to 2 were set as further parameters. The interpretation and visualization of results obtained from MaxQuant software were performed by a two-sample *t*-test using Perseus (v1.6.1.3, Max Planck Institute of Biochemistry, Germany). Statistical parameters ($p < 0.05$; $q < 0.05$, q = FDR adjusted p-value) were set to identify the differentially expressed proteins between samples (log_2 fold changes). The proteins were selected with a minimum of two peptides. Variability of biological replicates were measured using the scatter plot with Pearson correlation coefficient values of the LFQ intensities. The network protein analysis related to significantly altered proteins was carried out by Ingenuity Pathways Analysis (last release; Qiagen) based on Gene Ontology database. The statistical enrichment of involved pathways is performed by the right-tailed Fisher's exact test, in correlation with QIAGEN Knowledge Base, assigning a p-value (https://digitalinsights.qiagen.com/products/features/analysis-match/). The significance indicates the probability of association of molecules from the experimental dataset with the pathway by random chance alone. The overall activation/inhibition states of canonical pathways are predicted based on a z-score algorithm. The pathways are colored to indicate their activation z-scores: orange predict a gain of function, while blue a loss of function.

3. Results and discussion

The objectives of this study were to analyze whether and how carnosine prevents the modifications of skin proteome evoked by the exposure of hairless mice to UV-A. For this purpose, the skin samples recovered from Negre-Salvayre's previous study showing that UV-A generate lipid peroxidation products (HNE, carnosine) in the skin dermis of hairless mice chronically exposed to UV-A, and their

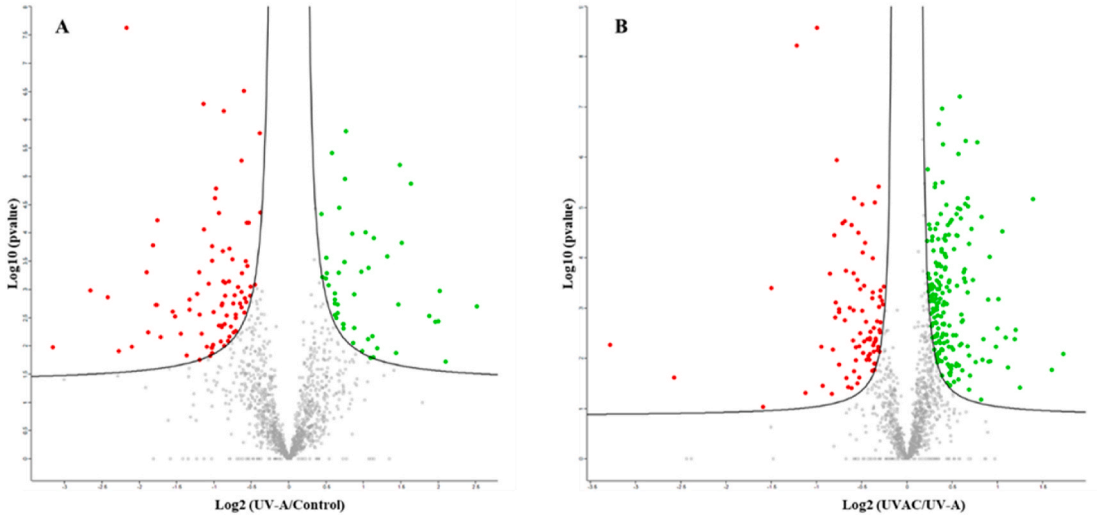

Fig. 1. Distribution of differentially regulated proteins induced by a) UV-A exposure vs Control, b) UV-A exposure w/wo carnosine. Green color indicates up-regulation (log_2 ratio ≥ 0.6), red color represents down-regulation (log_2 ratio ≤ -0.6); Scatter plots of log_2 ratio on x-axis against $-log_{10}$ p-value on y-axis of significantly quantified proteins (Perseus v 1.6.1.3). (For interpretation of the references to color in this figure legend, the reader is referred to the Web version of this article.)

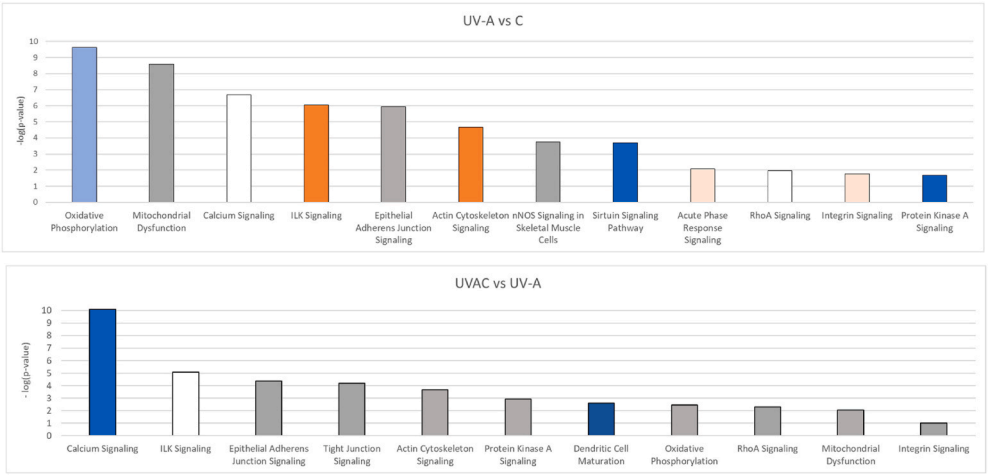

Fig. 2. Firsts canonical pathways obtained comparing a) UV-A vs Control and b) UVAC vs UV-A (IPA). In orange, increased pathways (positive z-score), in blue, decreased pathways (negative z-score), in white, no change (zero as z-score), in grey uncertain changes (NA z-score). (For interpretation of the references to color in this figure legend, the reader is referred to the Web version of this article.)

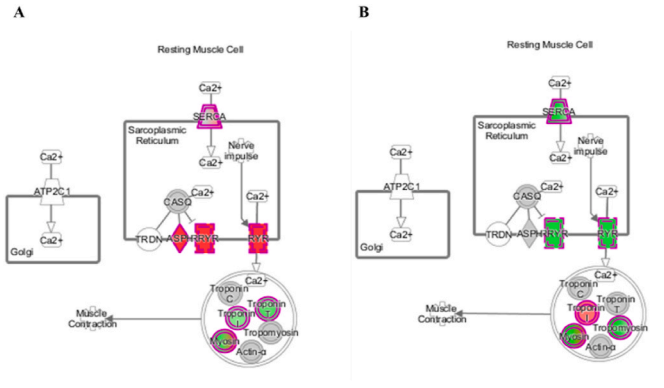

Fig. 3. Calcium signaling pathway enhanced in a) UV-A vs control and decreased in b) UVAC vs UV-A (IPA). In red the increased genes, in green those decreased. (For interpretation of the references to color in this figure legend, the reader is referred to the Web version of this article.)

prevention by a topical application of carnosine [10]. Skin samples were analyzed by applying a high-resolution mass spectrometry (MS)-based label-free quantitative (LFQ) proteomic technique, which first led to quantify a total of 2480 proteins, whose expression has been compared for each condition.

This technique allowed to identify 89 proteins significantly altered by UV-A exposure *vs* control (n = 30 up-regulated, 59 down-regulated) (Fig. 1A). Likewise, 252 proteins were identified in UV-A plus carnosine (UVAC) *vs* UV-A without carnosine (UVA) (n = 173 up-regulated, 79 down-regulated; Fig. 1B). Multi-scatter plots confirmed the quality and reproducibility of biological and technical replicates (Pearson correlation coefficient values ≥ 0.98). In the Supplementary Table 1, we present the complete list of quantified proteins obtained by MaxQuant software [29].

The identification and quantification of proteins differentially regulated for each condition (control, UVAC, UV-A) were followed by an analysis of the protein network, to describe the functional modules and pathways altered by UV-A radiations *w/wo* carnosine. In Fig. 2, we show

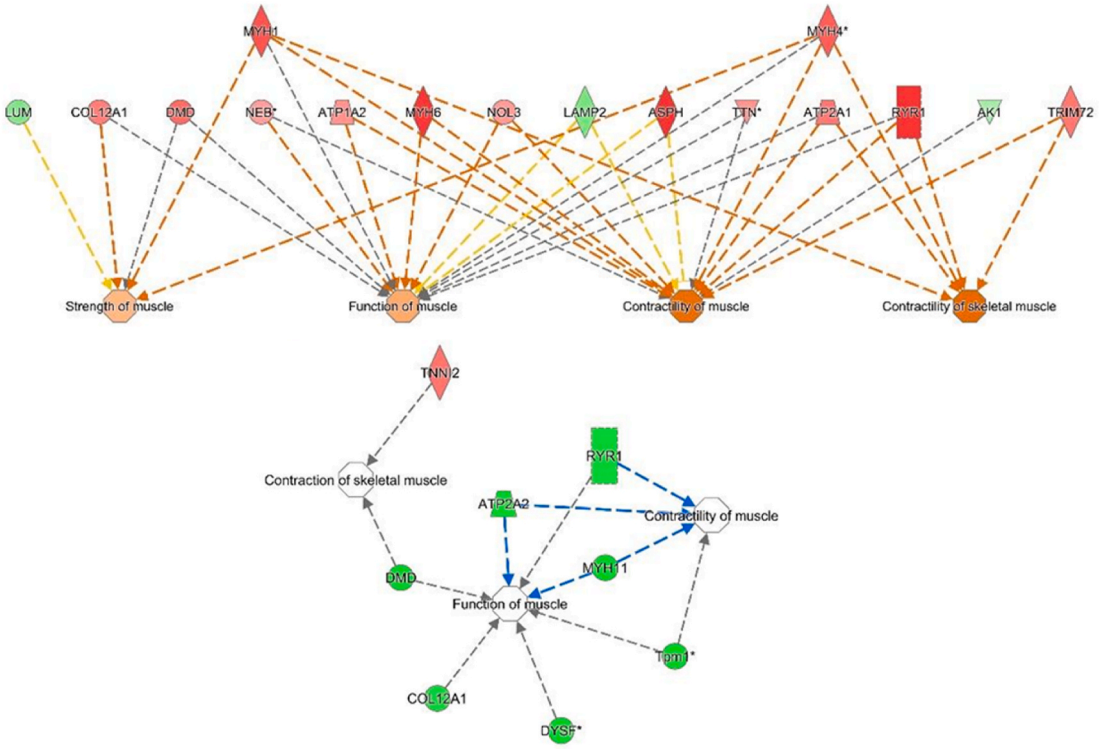

Fig. 4. Contraction related pathways in a) UV-A vs Control and b) UVAC vs UV-A. In red the increased genes, in green those decreased. The color intensity is positively related to the up- or down-gene's regulation; orange line leads to activation, blue lines lead to deactivation, yellow lines for findings inconsistent with state of downstream molecule, grey line for effect not predicted. (For interpretation of the references to color in this figure legend, the reader is referred to the Web version of this article.)

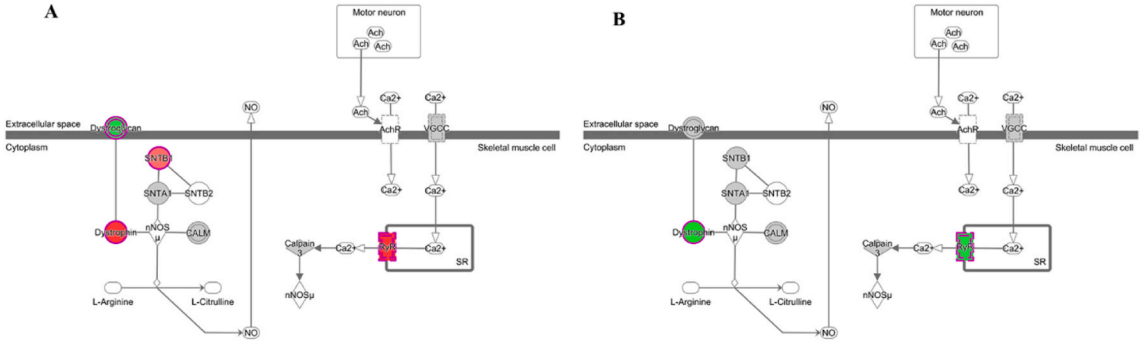

Fig. 5. nNOS signaling pathway enhanced in A) UV-A vs Control, B) decreased in UVAC vs UV-A (IPA). In red the increased genes, in green those decreased. (For interpretation of the references to color in this figure legend, the reader is referred to the Web version of this article.)

the most prominent canonical pathways obtained by Ingenuity Pathways Analysis (IPA) comparing UVA *vs* control (Fig. 2A) and UVAC *vs* UVA (Fig. 2B). The functional modules are based on statistical analyses and are associated with a p value and scores. In addition, the protein expression in each module was correlated with literature databases to predict the de/activation of the functional or disease modules. See the Supplementary Table 2 for the complete list of networks and related proteins.

3.1. Changes of skin dermis proteome evoked by UV-A exposure

Several pathways were severely altered by UV-A exposure, among them oxidative phosphorylation (p-value = 2.48 e^{-10}), mitochondrial dysfunction (p-value = 2.54 e^{-09}), integrin-linked kinase (ILK) signaling (p-value = 8.66 e^{-07}) and contraction as evidenced by the increase of calcium signaling (p-value = 1.96 e^{-07}; Fig. 3A), contractile and strength of muscular tissue pathway (p-value = 6.91 e^{-07}; Fig. 4), nNOS signaling (p-value = 1.80 e^{-07}; Fig. 5A), fibrogenesis and filaments formation (p-value = 5.83 e^{-06}; Fig. 6A).

Indeed, a significant increase could be observed for several cytoskeletal and contractile proteins or complexes such as dystrophin (DMD, $\log_2$ ratio = 0.99), keratin 31 (KRT31, $\log_2$ ratio = 2.00), myosin heavy chain 11 (MYH11, $\log_2$ ratio = −0.82) or ryanodine receptor (RyR-1, $\log_2$ ratio = −0.75) (Table 1, Supplementary Table 1).

Ryanodine receptor 1 (RyR-1) is expressed at the more external layer of the epidermis in the keratinocyte and has a role in barrier homeostasis [30]. RyRs are also actively involved in the regulation of intracellular calcium levels. In particular, the inhibition of RyR-1 was shown to accelerate the barrier recovery of the skin in the presence of wounds [31]. RyR-1 is not the unique regulator of calcium signaling altered by UV-A. Indeed, upon UV-A exposure we also observed a significant up-regulation related to aspartate beta hydroxylase (ASPH, $\log_2$ ratio =

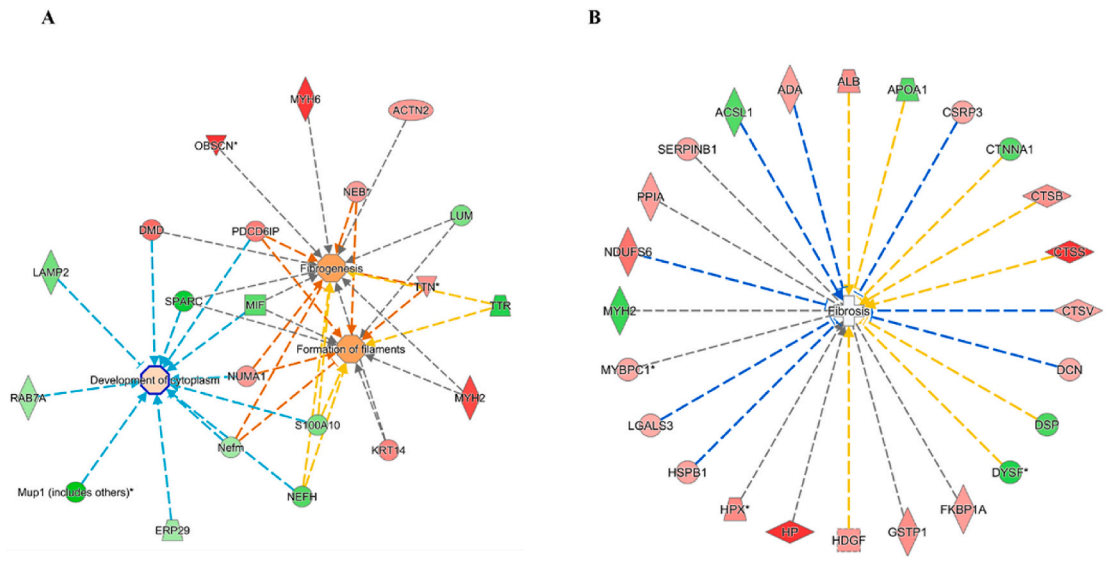

Fig. 6. Fibrosis related pathways in A) UV-A vs Control and B) UVAC vs UV-A. In red the increased genes, in green those decreased. The color intensity is positively related to the up- or down-gene's regulation; orange line leads to activation, blue lines for deactivation, yellow lines for findings inconsistent with state of downstream molecule, grey line for effect not predicted. (For interpretation of the references to color in this figure legend, the reader is referred to the Web version of this article.)

−2.10), involved in calcium homeostasis as well further than different isoforms of heavy chain of myosin involved in calcium binding and contraction, and DMD, a myosin binding protein. Moreover, the overexpression of myosin was related to fibrosis, showed by the accumulation of collagens, such as collagen alpha-1 (XII) chain (col12a1, $\log_2$ ratio = 0.87) and by the alteration of growth factor expression, regulated by integrin-linked kinase (ILK) pathway (z score = 1.90). The fibrotic process indeed is physiologically linked with the calcium signaling regulation as well as with the cell's damage induced, in this case, by UV-A. At this regard, calcium signaling has shown an active role on the inflammasome activation leading to fibrotic pathways (Carol et al., 2015).

Homeostasis of calcium regulates also the nNOS activity and its interaction with DMD, affecting NO signaling. On the skin, UVA radiation induced an upregulation of DMD ($\log_2$ ratio = 0.99) and Beta-1-syntrophin ($\log_2$ ratio = 0.68), the adapter protein involved in the formation of dystrophin glycoprotein complex. DAD1, dystrophin-associated glycoprotein 1 was highly down-expressed ($\log_2$ ratio = −0.701). The deregulation of nNOS signaling was also attested by the upregulation of RyR1 (Fig. 5A).

On the contrary, epithelial adherens junction signaling (p-value = 1.18 e^{-06}), immune response especially mediated by monocytes (p-value = 3.73 e^{-03}) and phagocytosis (p -value = 4.44 e^{-03}) were decreased related to controls. The two isoforms SH3 domain binding glutamate rich protein (SH3BGR and SH3BGRL3), belonging to thioredoxin like protein superfamily and involved in the redox homeostasis were also downregulated, indicating an impairment of ROS related pathways [32]. The metabolism of ROS was also down-regulated (p-value = 4.43 e^{-03}) (Supplementary Table 1).

Interestingly, sirtuin signaling was severely decreased upon UV-A treatment related to controls (p-value = 2.47 e^{-02}), suggesting an alteration of sirtuin activity and the turnover of acetylated proteins. These data agree with our recent report showing a decreased expression of the sirtuin SIRT1 in skin samples of hairless mice, and in dermis fibroblasts exposed to UV-A, directed related with photoaging [10]. Sirtuins are nicotinamide dinucleotide (NAD+)-dependent deacylases, able to stabilize the chromatin structure and histone diacylation, and promote the repair of DNA double-strand breaks [33,34]. Sirtuins may protect against photoaging [35], by inhibiting the expression and activity of metalloproteases (MMPs) and the degradation of collagen, while their knockdown, (particularly SIRT1) increases the levels of MMP-1 and -3 [34].

Overall, these results indicate that cell environment has been compromised (p-value range = 6.89 e^{-07} to 3.54 e^{-13}) as suggested by an alteration of several processes for instance related to cytoskeletal assembly and organization (p-value range = 6.89 e^{-03} to 4.90 e^{-12}), cell morphology (p-value range = 6.89 e^{-03} to 6.51 e^{-07}), energy production (p-value range = 6.89 e^{-03} to 7.23 e^{-07}) or nucleic acid metabolism (p-value range = 6.89 e^{-03} to 7.23 e^{-07}).

3.2. Effect of carnosine on skin proteome evoked by UV-A exposure

The treatment by carnosine prevented almost all conditions substantially altered by single UV-A exposure. Indeed, we found a reactivation of oxidative phosphorylation (p value = 2.59 e^{-03}) with an up regulation of Cytochrome C oxidase 6B1 (Cox6b1, $\log_2$ ratio = 1.25) and NADH ubiquinone oxidoreductase S8 ($\log_2$ ratio = 0.92), improving the functionality of mitochondria (p-value = 9.06 e^{-03}). In addition, we observed a decrease of calcium signaling (p-value = 8.73 e^{-11}; Fig. 3B), fibrosis (p-value = 1.99e-^{08}; Fig. 6B), cell migration (p-value = 2.27 e^{-03}) and nNOS pathway (p-value = 4.75 e^{-03}; Fig. 5B). We also found an increase of integrin-linked kinase (ILK) and actin signaling (p-value = 8.18 e^{-06}; 2.19 e^{-04} respectively), epithelial adherens junctions signaling (p-value = 4.05 e^{-05}), immune response mediated by neutrophils and leukocyte migration (p-value = 2.60 e^{-04}), attesting the regulation of signal transduction mediated by integrins and activation of immunity system.

Carnosine treatment was able to repristinate calcium homeostasis. Proteins related to contraction and fibrotic processes such as DMD ($\log_2$ ratio = −0.85) or MYH11 ($\log_2$ ratio = −0.82) were reduced (Table 1). RYR1 ($\log_2$ ratio = −0.75), sarcoplasmic/endoplasmic reticulum calcium ATPase (2Atp2a2, $\log_2$ ratio = −0.80) and calcium/calmodulin-dependent protein kinase II subunit gamma (Camk2g, $\log_2$ ratio = −0.78) as support of calcium channel's block (Table 1), were also significantly down-regulated. The reduction of fibrosis (Fig. 6B) and the regulation of NO signaling evoked by carnosine treatment were associated with a reversion of DMD and dystroglycan 1 expression (DAG1, $\log_2$ ratio = 0.35). The cellular organization and growth were enhanced (1.09e-^{08} to 4.43 e^{-08} and 9.98 e^{-03} to 1.83 e^{-05} as p value range, respectively) as well as function and maintenance (p-value range = 7.50

Table 1
Top up-/down-regulated proteins by UV-A or UVAC exposure involved in calcium signaling and fibrogenesis processes.

Gene name	Protein name	UniProt/ Swiss-Prot Accession	UVA vs C Log_2 Ratio	UVAC vs UVA Log_2 Ratio	Functional module
ATP2A2	ATPase sarcoplasmic/ endoplasmic reticulum Ca2+ transporting 2	Q5DTI2	0,16	−0,80	Ca^{2+} signaling
ATP2A3	ATPase sarcoplasmic/ endoplasmic reticulum Ca2+ transporting 3	Q8C213	0,84	−0,69	Ca^{2+} signaling
CAMK2G	calcium/ calmodulin dependent protein kinase II gamma	Q6ZWS7	0,60	−0,78	Ca^{2+} signaling
MYH11	myosin heavy chain 11	A0A338P6K2	−0,05	−0,82	Ca^{2+} signaling
MYL3	myosin light chain 3	P09542	NaN	1,00	Ca^{2+} signaling
MYL9	myosin light chain 9	Q9CQ19	−0,78	0,73	Ca^{2+} signaling
RYR1	ryanodine receptor 1	K3W4M2	2,52	−0,75	Ca^{2+} signaling
TNNI2	troponin I2, fast skeletal type	A2A6K0	−0,85	0,64	Ca^{2+} signaling
Tpm1	tropomyosin 1, alpha	A0A2R2Y2P8	−0,45	−1,12	Ca^{2+} signaling
MYH2	myosin heavy chain 2	G3UW82	1,18	−0,79	Ca^{2+} signaling/ fibrogenesis
ACTN2	actinin alpha 2	Q9JI91	0,68	0,03	fibrogenesis
DMD	Dystrophin	P11531	0,99	−0,85	fibrogenesis
KRT14	keratin 14	Q61781	0,82	−0,07	fibrogenesis
LUM	lumican	P51885	−0,90	0,11	fibrogenesis
MIF	macrophage migration inhibitory factor	Q545F0	−1,10	0,33	fibrogenesis
MYH6	myosin heavy chain 6	B2RQQ1	1,28	−0,59	fibrogenesis
NEB	nebulin	A2AQB2	0,65	−0,53	fibrogenesis
NEFH	neurofilament heavy	Q80TQ3	−1,14	0,33	fibrogenesis
Nefm	neurofilament, medium polypeptide	P08553	−0,65	0,26	fibrogenesis
NUMA1	nuclear mitotic apparatus protein 1	E9Q7G0	0,69	−0,42	fibrogenesis
OBSCN	obscurin, cytoskeletal calmodulin and titin-interacting RhoGEF	A2AAJ9	1,88	−0,49	fibrogenesis
PDCD6IP	programmed cell death 6 interacting protein	Q9WU78	0,85	−0,08	fibrogenesis
S100A10	S100 calcium binding protein A10	Q3UF30	−0,89	0,09	fibrogenesis
SPARC	secreted protein acidic and cysteine rich	Q5NCU4	−1,55	0,58	fibrogenesis
TTN	titin	A2ASS6	0,73	−0,49	fibrogenesis
TTR	transthyretin	Q9D6A4	−1,34	0,09	fibrogenesis

e−03 to 2.55 e−05). At this regard, proteins involved in nuclear functions, energetic metabolism, or reduction of oxidative stress as well as complement factor D (CFD, log2 ratio 1.39), glyceraldehyde-3-phosphate dehydrogenase (GAPCP2, log_2 ratio = 1.73) or Cox6b1 (log_2 ratio = 1.25) were significantly up-regulated (Supplementary Table 1). The thioredoxin like protein superfamily (SH3BGR and SH3BGRL3) were overexpressed after carnosine treatment, showing the regulation of redox homeostasis. Overall, these data confirm the benefit of a preventive carnosine treatment on cell and skin recovery after the UV-A injury.

Note that sirtuin signaling was partially improved by carnosine acting on genes' expression such as NDUFS8 (UVA vs C difference = -1.90 vs 0.91 in carnosine treatment) or NDUFA4 (−0.77 vs 0.33 as difference), in agreement with our recent observation showing that carnosine restores sirtuin activity in skin fibroblasts exposed to UV-A radiations [12].

Despite the use of murine model has greatly contributed also to the dermatological research, interspecies differences with humans must be considered to properly interpret the results. Among them, skin thickness, immunologic response, mechanism of contraction [36]. Moreover, a recent gene array study demonstrated as the most conserved skin genes between mice and humans are related to barrier structure or function, structure (cell-to-cell junctions), cell proliferation and communication [37]. Nevertheless, the use of hairless mice allowed us to mimic human skin UV-A response more accurately compared to unmodified models. Indeed, intrinsic and extrinsic skin damages to hairless mice are similar to that of humans [38]; Peres, P. S., 2011 [39]).

4. Conclusions

In conclusion, this study describes a high-resolution mass spectrometry (MS)-based label-free quantitative (LFQ) proteomic analysis of UV-A exposed murine skin and the effect of carnosine. We show here that several major protein systems are altered by UV-A treatment including calcium signaling, mitochondrial function or sirtuin expression, which were all restored by a preventive treatment of the skins by a topical application of carnosine. These results suggest that proteomics alterations could result (at least in part) from ROS generated by UV-A (and inhibited by carnosine), or/and the generation of lipid oxidation products (HNE, acrolein) resulting from the peroxidation of polyunsaturated fatty acids in the irradiated skins. These agents post-translationally modify proteins by forming adducts on free amino groups and thiol residues, which progressively alters protein expression and function, and trigger inflammatory and apoptotic responses [40–44]. The implication of such agents is emphasized by the potent efficacy of carnosine in restoring a normal proteomic profile of UV-A-treated skins, in accordance with its ability to neutralize the formation of adducts on proteins ad their subsequent modification, thereby restoring their function [16,45]. Beyond these observations, the high sensitivity of our proteomics approach should enable future analyses of murine or human skin, to check the protective potential of agents able to prevent or delay the mechanism of photoaging.

Declaration of competing interest

The authors state no conflict of interest.

Acknowledgements

We thank UNITECH OMICs, mass spectrometry platform of Università degli Studi di Milano, for running mass spectrometry analyses. We thank University of Milan for the PhD support grant.

Appendix A. Supplementary data

Supplementary data to this article can be found online at https://doi.

org/10.1016/j.freeradbiomed.2021.07.010.

References

[1] M. Berneburg, H. Plettenberg, J. Krutmann, Photoaging of human skin, Photodermatol. Photoimmunol. Photomed. 6 (2000) 239–244.
[2] G.J. Fisher, The pathophysiology of photoaging of the skin, Cutis 75 (2 Suppl) (2005) 5–8, discussion 8-9.
[3] M. Yaar, Gilchrest B.A. Aging versus photoaging: postulated mechanisms and effectors, J. Invest. Dermatol. Symp. Proc. 3 (1998) 47–51.
[4] M. Zhang, T. Zhang, Y. Tang, G. Ren, Concentrated growth factor inhibits UVA-induced photoaging in human dermal fibroblasts via the MAPK/AP-1 pathway, Biosci. Rep. 40 (2020) 7.
[5] E.C.C. Lan, Y.T. Hung, A.H. Fang, C.S. Wu, Effects of irradiance on UVA-induced skin aging, J. Dermatol. Sci. 94 (1) (2019) 220–228.
[6] J. D'Orazio, S. Jarrett, A. Amaro-Ortiz, T. Scott, UV radiation and the skin, Int. J. Mol. Sci. 14 (6) (2013) 12222–12248.
[7] B.A. Gilchrest, Photoaging. J Invest Dermatol. 133 (E1) (2013) E2–E6.
[8] M. Rinnerthaler, J. Bischof, M.K. Streubel, A. Trost, K. Richter, Oxidative stress in aging human skin, Biomolecules 21 (2015) 545–589.
[9] K.E. Burke, Photoaging: the role of oxidative stress, G. Ital. Dermatol. Venereol. 145 (2008) 445–459.
[10] P. Larroque-Cardoso, C. Camaré, F. Nadal-Wollbold, M.H. Grazide, M. Pucelle, S. Garoby-Salom, et al., Elastin modification by 4-hydroxynonenal in hairless mice exposed to UV-A. Role in photoaging and actinic elastosis, J. Invest. Dermatol. 135 (7) (2015) 1873–1881.
[11] J.H. Rabe, A.J. Mamelak, P.J. McElgunn, W.L. Morison, D.N. Sauder, Photoaging: mechanisms and repair, J. Am. Acad. Dermatol. 55 (1) (2006) 1–19.
[12] A. Swiader, C. Camaré, P. Guerby, R. Salvayre, A. Negre-Salvayre, 4-Hydroxynonenal contributes to fibroblast senescence in skin photoaging evoked by UV-A radiation, Antioxidants 10 (3) (2021) 365.
[13] R. Pandel, B. Poljšak, A. Godic, R. Dahmane, Skin photoaging and the role of antioxidants in its prevention, ISRN Dermatol 2013 (2013) 930164.
[14] M.C.B. Hughes, G.M. Williams, H. Pageon, A. Fourtanier, A.C. Green, Dietary antioxidant capacity and skin photoaging: a 15-year longitudinal study, J. Invest. Dermatol. 141 (4S) (2021) 1111–1118.e2.
[15] A. Altomare, G. Baron, E. Gianazza, C. Banfi, M. Carini, G. Aldini, Lipid peroxidation derived reactive carbonyl species in free and conjugated forms as an index of lipid peroxidation: limits and perspectives, Redox Biol 17 (2021) 101899.
[16] G. Aldini, R.M. Facino, G. Beretta, M. Carini, Carnosine and related dipeptides as quenchers of reactive carbonyl species: from structural studies to therapeutic perspectives, Biofactors 24 (2005) 77–87.
[17] G. Aldini, M. Carini, K.J. Yeum, G. Vistoli, Novel molecular approaches for improving enzymatic and nonenzymatic detoxification of 4-hydroxynonenal: toward the discovery of a novel class of bioactive compounds, Free Radic. Biol. Med. 69C (2014) 145–156.
[18] N.L. Anderson, N.G. Anderson, Proteome and proteomics: new technologies, new concepts, and new words, Electrophoresis 19 (11) (1998) 1853–1861.
[19] V. Dhingra, M. Gupta, T. Andacht, Z.F. Fu, New frontiers in proteomics research: a perspective, Int. J. Pharm. 299 (1–2) (2005) 1–18.
[20] B. Domon, R. Aebersold, Options and considerations when selecting a quantitative proteomics strategy, Nat. Biotechnol. 28 (7) (2010) 710–721.
[21] C.M. Huang, C.A. Elmets, K.R. van Kampen, T.S. De silva, S. Barnes, H. Kim, et al., Prospective highlights of functional skin proteomics, Mass Spectrom. Rev. 24 (5) (2005) 647–660.
[22] B. Dyring-Andersen, M.B. Løvendorf, F. Coscia, A. Santos, L.P. Møller, A.R. Colaço, et al., Spatially and cell-type resolved quantitative proteomic atlas of healthy human skin, Nat. Commun. 11 (2020) 5587.
[23] G. Fredman, L. Skov, M. Mann, B. Dyring-Andersen, Towards precision dermatology: emerging role of proteomic analysis of the skin, Dermatology (2021), https://doi.org/10.1159/000516764.
[24] L. Trilla-Fuertes, A. Gámez-Pozo, G. Prado-Vázquez, A. Zapater-Moros, M. Díaz-Almirón, C. Fortes, et al., Melanoma proteomics suggests functional differences related to mutational status, Sci. Rep. 9 (1) (2019) 7217.
[25] T. Agner, P. Elsner, Hand eczema: epidemiology, prognosis and prevention, J. Eur. Acad. Dermatol. Venereol. 34 (Suppl 1) (2020 Jan) 4–12.
[26] E. Szél, R. Bozó, É. Hunyadi-Gulyás, M. Manczinger, K. Szabó, L. Kemény, et al., Comprehensive proteomic analysis reveals intermediate stage of non-lesional psoriatic skin and points out the importance of proteins outside this trend, Sci. Rep. 9 (1) (2019) 11382.
[27] A. Srivastava, E. Barth, M.A. Ermolaeva, M. Guenther, C. Frahm, M. Marz, O. W. Witte, Tissue-specific gene expression changes are associated with aging in mice, Dev. Reprod. Biol. S1672–0229 (20) (2020) 30133–30139.
[28] Q. Qi, Q. Li, H. Zhu, H. Lu, X. Yang, Y. Wu, C. Feng, C. Fan, H. Li, B. Wu, Y. Gao, Z. Zhang, H. Zhou, J. Zuo, W. Tang, Triptolide analog LLDT-8 ameliorates psoriasis-like dermatitis in BALB/c mice via suppressing the IL-36α signaling pathway, Pharmacol. Res. 169 (2021) 105678.
[29] J. Cox, M.Y. Hein, C.A. Luber, I. Paron, N. Nagaraj, M. Mann, Accurate proteome-wide label-free quantification by delayed normalization and maximal peptide ratio extraction, termed MaxLFQ, Mol. Cell. Proteomics 13 (9) (2014) 2513–2526.
[30] S. Denda, J. Kumamoto, K. Takei, M. Tsutsumi, H. Aoki, M. Denda, Ryanodine receptors are expressed in epidermal keratinocytes and associated with keratinocyte differentiation and epidermal permeability barrier homeostasis, J. Invest. Dermatol. 132 (1) (2012 Jan) 69–75.
[31] D. Degovics, P. Hartmann, I.B. Németh, N. Árva-Nagy, E. Kaszonyi, E. Szél, et al., A novel target for the promotion of dermal wound healing: ryanodine receptors, Toxicol. Appl. Pharmacol. 366 (2019) 17–24.
[32] M. Mazzocco, M. Maffei, A. Egeo, A. Vergano, P. Arrigo, R. Di Lisi, et al., The identification of a novel human homologue of the SH3 binding glutamic acid-rich (SH3BGR) gene establishes a new family of highly conserved small proteins related to Thioredoxin Superfamily, Gene 291 (1–2) (2002) 233–239.
[33] B.J. North, Verdin E. Sirtuins, Sir2-related NAD-dependent protein deacetylases, Genome Biol. 5 (5) (2004) 224.
[34] S.H. Lee, J.H. Lee, H.Y. Lee, K.J. Min, Sirtuin signaling in cellular senescence and aging, BMB Rep 52 (1) (2019) 24–34.
[35] L.M. Garcia-Peterson, M.J. Wilking-Busch, et al., Sirtuins in skin and skin cancers, Skin Pharmacol. Physiol. 30 (4) (2017) 216–224.
[36] H.D. Zomer, A.G. Trentin, Skin wound healing in humans and mice: challenges in translational research, J. Dermatol. Sci. 90 (1) (2018 Apr) 3–12, https://doi.org/10.1016/j.jdermsci.2017.12.009.
[37] P.A. Gerber, B.A. Buhren, H. Schrumpf, B. Homey, A. Zlotnik, P. Hevezi, The top skin-associated genes: a comparative analysis of human and mouse skin transcriptomes, Biol. Chem. 395 (2014) 577–591.
[38] C.F. Hung, C.L. Fang, S.A. Al-Suwayeh, S.Y. Yang, et al., Evaluation of drug and sunscreen permeation via skin irradiated with UVA and UVB: comparisons of normal skin and chronologically aged skin, J. Dermatol. Sci. 68 (2012) 135–148.
[39] P.S. Peres, V.A. Terra, F.A. Guarnier, R. Cecchini, A.L. Cecchini, Photoaging and chronological aging profile: understanding oxidation of the skin, J. Photochem. Photobiol., B 103 (2011) 93–97.
[40] F. Guéraud, M. Atalay, N. Bresgen, A. Cipak, P.M. Eckl, L. Huc, et al., Chemistry and biochemistry of lipid peroxidation products, Free Radic. Res. 44 (10) (2010) 1098–1124.
[41] P. Jørgensen, L. Milkovic, N. Zarkovic, G. Waeg, S.I.S. Rattan, Lipid peroxidation-derived 4-hydroxynonenal-modified proteins accumulate in human facial skin fibroblasts during ageing in vitro, Biogerontology 15 (1) (2014) 105–110.
[42] G. Vistoli, D. De Maddis, A. Cipak, N. Zarkovic, M. Carini, G. Aldini, Advanced glycoxidation and lipoxidation end products (AGEs and ALEs): an over-view of their mechanisms of formation, Free Radic. Res. 47 (Suppl 1) (2013) 3–27.
[43] H. Zhang, H.J. Forman, 4-hydroxynonenal-mediated signaling and aging, Free Radic. Biol. Med. 111 (2017) 219–225.
[44] N. Rabbani, P.J. Thornalley, Dicarbonyl stress in cell and tissue dysfunction contributing to ageing and disease, Biochem. Biophys. Res. Commun. 458 (2) (2015) 221–226.
[45] A.A. Boldyrev, G. Aldini, W. Derave, Physiology and pathophysiology of carnosine, Physiol. Rev. 93 (4) (2013) 1803–1845.